JTTEE5 11:393–399

Dynamic Hardness of Detonation Sprayed WC-Co Coatings

Manish Roy

(Submitted 18 January 2001; in revised form 16 May 2001)

The objective of the present work was to determine the dynamic hardness of WC-Co coatings from the dynamic hardness of the coating substrate system. It was also the purpose of this work to evaluate the influence of coating composition, coating thickness, and substrate materials on the dynamic hardness of the coating. To achieve the above-mentioned objectives, WC-12%Co and WC-17%Co coatings were deposited by detonation spraying on three different substrate materials: mild steel, commercially pure (CP) aluminum, and CP titanium. The dynamic hardness of the coating/substrate composite was evaluated by a drop weight system. The dynamic hardness of the coating independent of the substrate was determined from the dynamic hardness of the coating/substrate composite.

Keywords detonation spraying, dynamic hardness, high strain rate, volume law of mixture, WC-Co coatings

1. Introduction

One important mechanical property that governs the tribological behavior of coatings is their hardness. Reliable and reproducible hardness values of the coatings are determined by microindentation (load range 1-1000 g) or ultra microindentation (load range 0.1-10 g). When the coating contains a two-phase microstructure, with each phase having widely different mechanical properties, determination of hardness at the macro level (for a minimum load of 5000 g) will provide a more representative property than micro level. However, determination of hardness of coatings at the macro level without the influence of substrate is difficult. As a result, several attempts have been made to determine the hardness of the coating/substrate composite system and to separate the coating hardness from the hardness of the coating/substrate system.[1-3] One such attempt to determine hardness of thin films was made by Burnett and Rickerby[4] using the volume law of mixture.

The dynamic hardness of coatings simulates the deformation behavior of materials under tribological degradation conditions more accurately[5-7] than static hardness. Dynamic hardness of the coating substrate system is mentioned in Ref. 8. This dynamic hardness of the coatings independent of the influence of substrate is yet to be reported in the literature.

In view of the above, an attempt has been made to determine the dynamic hardness of a series of detonation sprayed WC-Co coatings using a drop weight system.[9] Determination of hardness with such a system is influenced by the substrate hardness. Hence, the volume law of mixture approach was used. Determination of dynamic hardness using a drop weight system involves deformation of a large volume of coating. Thus, hardness obtained by this method provides a more representative property of a material having two different phases (such as WC-Co) than the hardness obtained by microindentation at low load deforming a small volume.

Manish Roy, Defence Metallurgical Research Laboratory, P.O. Kanchanbagh, Hyderabad-500 058, India. Contact e-mail: manish@dmrl.ernet.in.

2. Experimental Details

2.1. Coatings

WC-12%Co and WC-17%Co powders were deposited on mild steel, commercially pure (CP) Ti, and CP Al. The micrograph of the powder used for detonation spraying is shown in Fig. 1. The particles are rounded and of 50 ± 25 μm average diameter. These sintered particles are manufactured by AMPERIT (Hermann C. Starck, Berlin, Germany). Detonation spraying was carried out with DNIPER-3 detonation gun (Institute of Material Science Problems, Ukraine), the details of which are given elsewhere.[10] Coating was deposited using the above gun at the International Advanced Research Centre for Powder Metallurgy and New Materials, Hyderabad, India.

2.2. The Gravity Drop System

A schematic view of the gravity drop system is shown in Fig. 2. The balls are released from the ball feeder system and allowed to drop freely under the influence of gravity. The target in the form of a flat sample is fixed rigidly to the target holder at the bottom. The orientation of the sample was always normal to the path of the impacting ball.

A velocity measurement system shown in Fig. 2 was used to measure the incident as well as the rebound velocity of the ball. The system consists of a timer, which can measure the time taken by the ball to cross the frame during incident as well as during rebound movement. Further details relating to measurement of impact and rebound velocity is available in Ref. 9.

3. Methods of Estimation

3.1. Determination of Coefficient of Restitution

The sensing frames of the velocity measuring units are separated by a distance X and the plane where the velocity is mea-

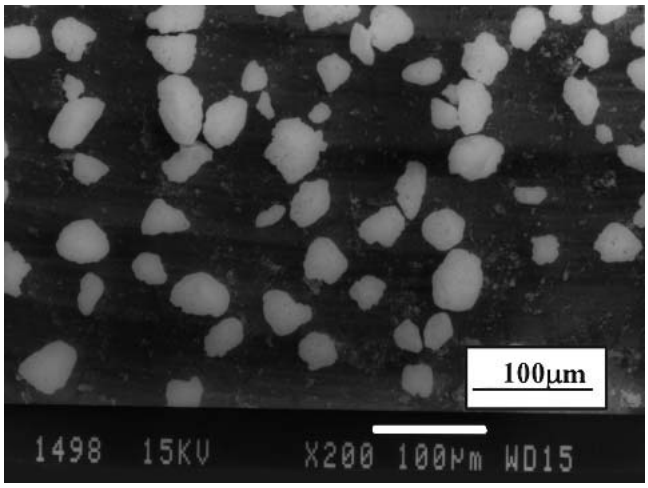

Fig. 1 SEM micrographs of the powders used for detonation sprayed coatings

sured is situated at a distance b from the top of the sample surface (Fig. 2). Thus, actual incident (V) and rebound (V_r) velocities can be estimated from the measured incident (V_m) and rebound (V_{rm}) velocities as

$$V^2 = V_m^2 + 2gb \quad \text{(Eq 1)}$$
$$V_r^2 = V_{rm}^2 + 2gb \quad \text{(Eq 2)}$$

where

$$V_m = \frac{X}{t_i} \text{ and } V_{rm} = \frac{X}{t_r} \quad \text{(Eq 3)}$$

Hence,

$$e = \frac{V_r}{V} = \frac{t_r}{t_i}\left(\frac{1 + Yt_i^2}{1 + Yt_r^2}\right)^{1/2} \quad \text{(Eq 4)}$$

In Eq 1-4, $Y = 2\ gb/X^2$, e is the coefficient of restitution, g is acceleration due to gravity, and t_i and t_r are the time taken by the ball to travel the frame during incident and rebound movements, respectively.

3.2. Determination of the Dynamic Hardness of the Coating/Substrate Composite Layer and Other Related Parameters

The coefficient of restitution (e) is related to the dynamic hardness (H_d) by [6]

$$e = 1.9H_d^{5/8}/E_e^{1/2}\rho_b V^{1/4} \quad \text{(Eq 5)}$$

Hence,

$$H_d = 0.53e^{8/5}E_e^{4/5}\rho_b^{1/5}V^{2/5} \quad \text{(Eq 6)}$$

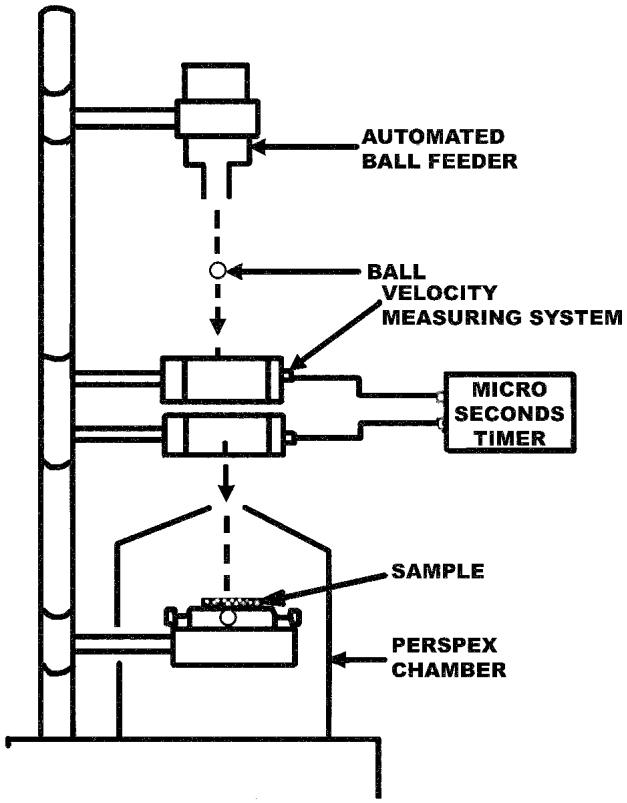

Fig. 2 Schematic representation of the gravity drop system

where ρ_b is the density of the ball, V is the impact velocity, and E_e is the effective elastic modulus, and is given as

$$E_e = E_b E_t/[(1 - \nu_b^2)E_t + (1 - \nu_t^2)E_b] \quad \text{(Eq 7)}$$

Here E_b, E_t, ν_b, and ν_t are elastic modulus and Poisson's ratio of the ball and the target materials, respectively.

The crater diameter (W) is related to the dynamic hardness by[9]

$$W = 2.56rV^{1/2}(\rho_b/H_d)^{1/4} \quad \text{(Eq 8)}$$

where r is the radius of the impacting ball and hence, depth of deform zone R is given by[11]

$$R = KW \quad \text{(Eq 9)}$$

where K is a constant and its value is between 1.25 and 1.5. The crater depth (d) is given by[11]

$$d = W^2/8r \quad \text{(Eq 10)}$$

3.3. Determination of the Dynamic Hardness of the Coating From the Dynamic Hardness of the Coating/Substrate Composite

The hardness of the coating was estimated from the hardness (H_{comp}) of the coating substrate composite by employing the volume law of mixture by Burnett and Rickerby[4] as

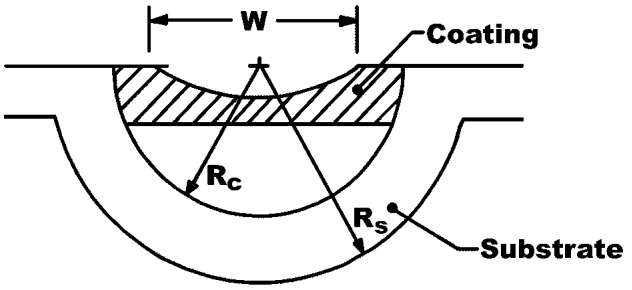

Fig. 3 Schematic view of the deformed zones in the coating and in the substrate

$$H_{comp} = \frac{V_c}{V} H_c + \frac{V_s}{V} H_s \quad \text{(Eq 11)}$$

where V_c, V_s, H_c, and H_s are the volume and hardness of the coatings and the substrate, respectively. V is the total volume. Because of the constraint at the interface, Eq 11 was further modified as

$$H_{comp} = \frac{V_c}{V} H_c + \frac{V_s}{V} \chi^3 H_s \quad \text{(Eq 12)}$$

where χ is the interface constraint and is given by[3]

$$\chi = \left(\frac{E_c H_s}{E_s H_c}\right)^{1/p} \quad \text{(Eq 13)}$$

where p is between 2 and 3. Ichimura et al.[12] further simplified this equation and produced the expression

$$H_{comp} = \frac{3}{2}\left(\frac{H_c R_c^2}{\chi^3 R_s^3} - \frac{H_s}{\chi R_s}\right) t + H_s \quad \text{(Eq 14)}$$

where R_c and R_s are the radius of the deformed zone in the coatings and substrate, respectively, as shown in Fig. 3, and t is the thickness of the coating. R_c and R_s can be expressed in terms of H_c and H_s using Eq 8 and 9. Hence, putting the value of R_c from Eq 8 and 9, Eq 14 is given as

$$H_{comp} = \frac{3}{2}\left(\frac{10.24 H_c^{1/2} r^2 V \rho_b^{1/2}}{\chi^3 R_s^3} - \frac{H_s}{\chi R_s^3}\right) t + H_s \quad \text{(Eq 15)}$$

Rearranging Eq 15, we get

$$H_c = \left\{\frac{0.065\ \chi^3 R_s^3}{r^2 V \rho_b^{1/2} t}(H_{comp} - H_s) + 0.098\frac{\chi^2 R_s}{r^2 V \rho_b^{1/2}}\right\}^2 \quad \text{(Eq 16)}$$

4. Results and Discussion

The scanning electron microscope (SEM) micrograph showing the morphology of the coated surface is shown in Fig. 4. The coated surface exhibits globular type morphology with some irregularly shaped lumps. A low magnification micrograph of the transverse section of the coating on mild steel substrate is presented in Fig. 5. No subsurface cracks in the coating can be seen. The coating thickness is approximately 200 μm. Figure 6 shows the high magnification SEM micrograph of the coating. Lenticular splats are deposited one after another in the coating. WC particles in the size range of 1-8 μm are dispersed throughout the coating. The microstructural features of WC-Co coating having slightly different composition and deposited on different substrates are nearly same, and hence are not reproduced for the sake of the brevity.

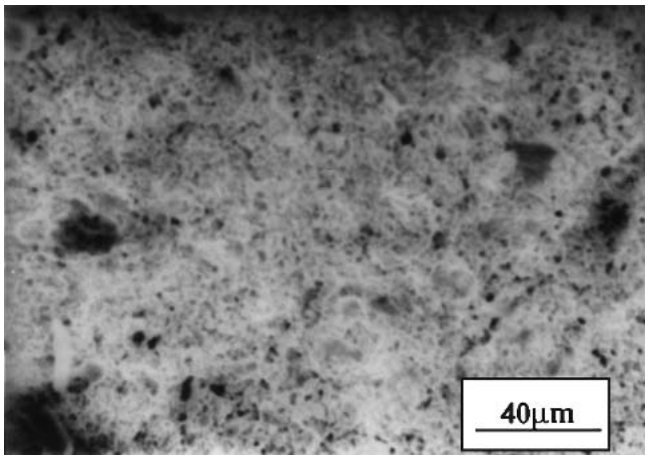

Fig. 4 SEM micrograph showing the morphology of the coated surface

The various coating/substrate combinations used in the present experiment along with the microhardness of the coatings, the elastic modulus, and effective elastic modulus are given in Table 1. Microhardness was carried out using a Knoop indenter at 30 g load and the corresponding hardness is given. Each reading is an average of five readings. The values of elastic modulus are collected from the literature.[13] The coefficient of restitution is determined experimentally employing Eq 1-4. Using these parameters and using equations described in previous section, the coefficient of restitution and dynamic hardness of the coating/substrate composites were determined (Table 2). Equations 9 and 10 were used to determine the depth of the deformed zones and the crater depth listed in Table 2. From Table 2, it is clear that coefficient of restitution (e) and dynamic hardness (H_d) are higher for the WC-12%Co coating/substrate system (sample numbers 1, 3, 4, and 6) than WC-17%Co coating/substrate system (sample numbers 2 and 5). e and H_d are also greater for thick coatings than thin coatings. Finally, e and H_d are greater for the system in which the substrate has a higher H_d value. All of the substrates have either higher or equal dynamic hardness than static hardness (Table 2).

Employing the principle of volume law of mixture and using Eq 11-16, the dynamic hardness of the coatings independent of the substrate influence were obtained. The interface constraint factors are obtained using static hardness of the substrate and the coating. The dynamic hardness of the coatings and the ratio of the dynamic to static hardness are presented in Table 3. Table 3 also contains the interfacial constraint factor χ, obtained through Eq 13. Thus, from Table 3, most of the coatings exhibit higher hardness at a higher strain rate. The hardness of the coating is

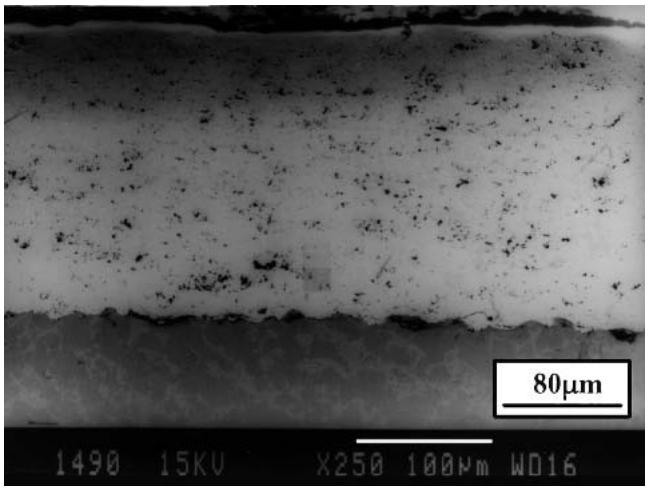

Fig. 5 Low magnification SEM micrograph of the sectioned surfaces of the WC-12%Co coatings

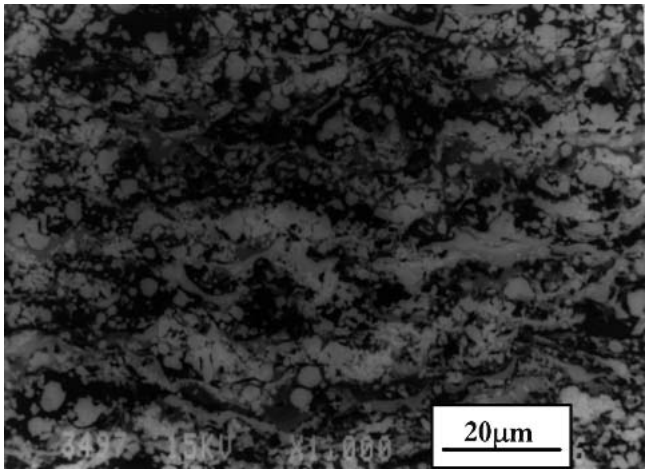

Fig. 6 High magnification SEM micrograph of the WC-12%Co coatings

influenced by the substrate coatings constraint factors. A WC-12%Co coating of 200 μm thickness on aluminum exhibits the highest dynamic hardness. In contrast, a WC-12%Co coating of 200 μm thickness on mild steel shows the minimum hardness. The dynamic hardness of a WC-12%Co coating is lower than that of a WC-17%Co coating on mild steel substrate. The dynamic hardness for both types of coating is lowest on mild steel substrate and highest on Al substrate. The dynamic hardness assumes an intermediate value on a Ti substrate. Dynamic hardness is higher on thinner coatings than on thicker coatings.

As noted in the present work, the dynamic hardness of a WC-17%Co coating on mild steel substrate is higher than that of WC-12%Co, even though static hardness shows the reverse trend. A WC-17%Co coating has more cobalt with a lower melting point than WC. This cobalt will be melted during spraying and can occupy micropores. Thus, this coating will have less micropores because of higher cobalt content than the WC-12%Co coating. Static hardness is measured at low load at the micro-level. The dynamic hardness is determined at the macro-level, which involves indenting and deforming much larger volumes or equivalently at higher loads. At low loads, material above the pores can withstand the load and the extent of compaction is less. At high loads, the extent of compaction is high. Materials above the pores are forced to occupy the micropores. Hence, the influence of micropores will not be reflected in the static microhardness values, which are conducted at low load, producing less compaction. However, this influence is reflected in the dynamic hardness, which is measured at macro-level. Hence, WC-17%Co coatings show higher hardness during dynamic indentation and lower hardness during static indentation. The influence of micropores is not reflected for the coating on aluminum substrate because of the presence of high residual stress. In other words, the increase of hardness because of residual stress in WC-Co coatings on aluminum is higher than the decrease of hardness because of the presence of micropores. Thus, on aluminum alloy, the WC-12%Co coating exhibits higher hardness than the WC-17%Co coating.

In this investigation it was also noted that substrate significantly influenced dynamic hardness. For the same coating, dynamic hardness on CP aluminum is highest and that on mild steel is lowest; dynamic hardness is intermediate on the Ti substrate. There are two reasons for the trend described above. One possible reason is the presence of residual stress. This stress is given as[14]

$$\sigma_s = \frac{E_s E_c \Delta T(\alpha_s - \alpha_c)}{E_s - E_c(t_c/t_s)} \quad \text{(Eq 17)}$$

where E_c, E_s, α_c, α_s, t_c, and t_s are the elastic modulus, thermal expansion coefficient, and thickness of the coatings and substrate, respectively. ΔT is the temperature difference experienced by powders on deposition. Because the thickness of the coating (200 μm) was very low compared with the thickness of the samples (8 mm) used in the present investigation, Eq 17 can be further simplified as

$$\alpha_s = E_c \Delta T(\alpha_s - \alpha_c) \quad \text{(Eq 18)}$$

Thus, for a given value of E_c and ΔT, the residual stress will depend on the differences of the thermal expansion coefficient between the coating and the substrate. α_c in the present case is around 5.2 μm/mK.[15] α_s values for Al, Ti, and mild steel are 25, 11.0, and 11.0 μm/mK, respectively. However, for CP Ti having hexagonal structure, the thermal expansion coefficient can be as high as 12.8 μm/mK in one crystallographic direction. Thus, $\alpha_s - \alpha_c$ will be maximum for Al, intermediate for Ti, and minimum for mild steel, giving rise to residual stress that will be maximum for Al, intermediate for Ti, and minimum for mild steel.

The second reason for the described trend is as follows. When Eq 11 is used, the deformed volume is estimated from depth of deformation (R), which is derived from Eq 9 as $R = 1.25W$ where, W is crater diameter. This is a very conservative estimation of depth of the deformed zone. During dynamic hardness measurement, the contact time between the impacting ball and the target material is very small (measured in microseconds). Hence, the heat generated due to impact does not get enough

Table 1 Various Coatings and Substrate Materials Tested in the Present Work Along With Their Modes of Elasticity and Hardness

Sample No.	Substrate	Coating	Thickness of Coating, μm	Elastic Modulus, Gpa	Effective Elastic Modulus, GPa	Hardness of Coating/Substrate, GPa (KHN)
1	Mild steel	WC-12%Co	200	232	170	10.2 (928 ± 20)
2	Mild steel	WC-17%Co	200	212	160	7.7 (754 ± 11)
3	Mild steel	WC-12%Co	50	232	170	10.2 (928 ± 20)
4	CP Al	WC-12%Co	200	232	170	10.2 (928 ± 20)
5	CP Al	WC-17%Co	200	212	160	7.7 (754 ± 11)
6	CP Ti	WC-12%Co	200	232	170	10.2 (928 ± 20)
7	Mild steel	…	…	208	162	2.2 (220 ± 8)
8	CP Al	…	…	62	61	0.9 (77.4 ± 2)
9	CP Ti	…	…	117	105	2.2 (208 ± 4)

Table 2 Coefficient of Restitution, Dynamic Hardness of Coating Substrate Combination, Depth of Deformed Zone, and Crater Depth

Sample No.	Substrate	Coating	Thickness of Coating, μm	Coefficient of Restitution	Dynamic Hardness, GPa	Depth of Deformed Zone, m	Crater Depth, m
1	Mild steel	WC12-%Co	200	0.57	4.6	1.88×10^{-3}	8.9×10^{-5}
2	Mild steel	WC-17%Co	200	0.57	4.4	1.90×10^{-3}	9.1×10^{-5}
3	Mild steel	WC-12%Co	50	0.42	2.4	2.21×10^{-3}	12.3×10^{-5}
4	CP Al	WC-12%Co	200	0.43	2.9	2.11×10^{-3}	11.2×10^{-5}
5	CP Al	WC-17%Co	200	0.38	2.3	2.24×10^{-3}	12.7×10^{-5}
6	CP Ti	WC-12%Co	200	0.66	5.9	1.78×10^{-3}	7.9×10^{-5}
7	Mild steel	…	…	0.35	2.0	2.3×10^{-3}	13.4×10^{-5}
8	CP Al	…	…	0.33	8.6	2.86×10^{-3}	20.7×10^{-5}
9	CP Ti	…	…	0.62	3.6	2.0×10^{-3}	10.1×10^{-5}

Table 3 Interface Constraint Factor, Dynamic Hardness, and the Ratio of the Dynamic to Static Hardness

Sample No.	Substrate	Coating	Thickness of Coating, μm	Interface Constraint Factor	Dynamic Hardness of Coating, GPa	Ratio of Dynamic to Static Hardness of Coatings
1	Mild steel	WC-12%Co	200	0.67	1.6	1.59
2	Mild steel	WC-17%Co	200	0.67	1.8	2.40
3	Mild steel	WC-12%Co	50	0.64	1.7	1.68
4	CP Al	WC-12%Co	200	0.69	4.7	4.59
5	CP Al	WC-17%Co	200	0.71	3.2	4.16
6	CP Ti	WC-12%Co	200	0.76	2.0	1.93

time to dissipate. This makes the deformation adiabatic. As material undergoes deformation, it becomes hardened because strain hardening and deformation tends to spread to the soft zone. Under adiabatic deformation conditions, and also under compression stress, the material beyond some strain will become softened because of thermal softening. This will lead to localization of deformation rather than spreading of the deformation. The critical strain required for localization of deformation is given as[16]

$$\varepsilon_c = \left(\frac{n\rho C_p}{3KC}\right)^{1/1+n} \quad \text{(Eq 19)}$$

where n is strain hardening exponent, ρ is the density, C_p is the specific heat, K is the strength coefficient, and C is the temperature coefficient of shear modulus of the material. The temperature coefficient of shear modulus is equal to $KT_M^{0.75}$, [17] where T_M is the melting point. Furthermore, the value of n decreases sharply as the strain approaches the critical strain for localization. This results in alteration of Eq 19[18].

$$\varepsilon_c = \frac{n\rho C_p T_M^{0.75}}{3K} \quad \text{(Eq 20)}$$

Thus, from Eq 20, the higher the melting point of the material, the higher is the strain required for localization. In other words, the lower the melting point of the material, the easier is the localization of deformation. For low melting materials like aluminum, the deformation tends to localize rather than spread. The depth of deformation obtained through Eq 9 is overestimated, particularly for low melting point aluminum, and this overestimation is minimum for high melting point mild steel. If the depth of deformation is taken as $1.25W$ rather than $1.5W$, the estimated dynamic hardness becomes nearly half. Thus, overestimation of the depth of deformation, and in turn deformed volume, is partly responsible for the high value of dynamic hardness, particularly for CP aluminum.

Table 4 The Average Strain, Time of Impact, and Average Strain Rates of Various Coatings/Substrate System and Substrate

Sample No.	Substrate	Coating	Thickness of Coating, μm	Average Strain	Time of Impact	Average Strain Rate, sec^{-1}
1	Mild steel	WC-12%Co	200	0.047	2.33×10^{-5}	2040
2	Mild steel	WC-17%Co	200	0.050	2.38×10^{-5}	2015
3	Mild steel	WC-12%Co	50	0.056	3.22×10^{-5}	1734
4	CP Al	WC-12%Co	200	0.053	2.91×10^{-5}	1822
5	CP Al	WC-17%Co	200	0.056	3.30×10^{-5}	1714
6	CP Ti	WC-12%Co	200	0.045	2.07×10^{-5}	2163
7	Mild steel	…	…	0.058	3.5×10^{-5}	1655
8	CP Al	…	…	0.072	5.4×10^{-5}	1334
9	CP Ti	…	…	0.050	2.6×10^{-5}	1895

Finally, dynamic hardness of thinner coatings is higher than that of thicker coatings. This phenomenon for thermal sprayed coating is not yet reported. This phenomenon is well demonstrated for physical vapor deposition (PVD) coatings.[19] A higher hardness for a thin NiO scale compared with thick NiO scale is also obtained.[20]

When the dynamic hardness (H_d) was calculated from the coefficient of restitution, the effective E was estimated for the coating and the impacting ball. The effective E is the combined E of the materials that are interacting during impact. The influence of the substrate on the effective E was ignored. An examination of crater depth in the WC-Co coatings shows that most of the crater has approximately 100 μm depth. Thus, there was no interaction between the impacting ball and substrate during impact. In contrast, coating thickness was around 200 μm. Only in one case was the coating 50 μm. Thus, the crater was very much within the coating. Hence, estimation of effective elastic modulus from coating and the impacting ball is enough because there was no interaction between the substrate and the impacting ball during impact.

Simplification of Eq 12 to Eq 14 was derived for a thin film coating, e.g., 10 μm thick coatings. In the present case, coating thickness was 200 μm. However, given the radius of the deformed zone in Al (2860 μm, Table 2) or even in mild steel (2300 μm, Table 2), 200 μm is still very thin. It becomes negligible when the square of the coating thickness is compared with the square of the depth of deformed zone.[12] In practice, the error introduced for a 200 μm thick coating in simplifying Eq 12 to Eq 14 is less than 5%.

During the estimation of the deformed volume, the crater volume is neglected. This is also expected to contribute some error. A typical example is considered here. In mild steel, the volume of the deformed zone is $2.22 \times 10^{-9} m^3$, with a crater of depth $2.6 \times 10^{-5} m$ and diameter of 5.4×10^{-4} m, producing a crater volume of $2.98 \times 10^{-12} m^3$. The crater volume is only 0.13% of the deformed volume and this is negligible. Hence, error due to the assumption that crater volume is negligible in comparison to deformed volume is nominal.

The interfacial constraint factor is determined using Eq 13 according to Bull and Rickerby.[3] These investigators experimentally found that the exponent on the right-hand side of Eq 13 is between 0.33 and 0.5. This observation was valid for thin film obtained by the PVD technique. In the present work, the coating was obtained by detonation spraying. In such thermal spraying with a relatively thick coating, the interfacial constraint is expected to be a little less compared with thin film obtained by the PVD technique. This is why the exponent of the right-hand side of the equation is assumed to be 0.33 instead of 0.5.

The deformation of materials under tribological degradation has certain unique features. One important feature is high strain rate deformation. Static hardness data that are used as governing parameters are obtained at a very low strain rate. In contrast, dynamic hardness data are obtained at a significantly higher strain rate.

Strain rate associated with dynamic hardness can be calculated as described below. The average strain (ε_{av}) for hardness measurement is given as[21]

$$\varepsilon_{av} = 0.1\frac{W}{r} \quad \text{(Eq 21)}$$

The time of contact (t_{im}) during impact is obtained as[22]

$$t_{im} = 1.28 r \rho_b^{1/2} / H_d^{1/2} \quad \text{(Eq 22)}$$

Thus, average strain rate (ε_{av}) can be obtained as ε_{av}/t_{im} or

$$\varepsilon_{av} = 0.2 V^{1/2} H_d^{1/4} / r \rho_b^{1/4} \quad \text{(Eq 23)}$$

The average strain, time of impact, and strain rates are summarized in Table 4. The average strain rates obtained for various coating substrate combinations varies between 1.3×10^3 and 2.1×10^3. These values are close to the strain rate at which most of the metals and alloys undergo abrasive wear, and are a little lower than the strain rate observed during erosive wear.[6] Thus, dynamic hardness is a more representative property than the static hardness of the coating to monitor the deformation behavior of the coating during tribological degradation.

5. Conclusions

- WC-Co coatings exhibit higher hardness under impact at high strain rate.
- The dynamic hardness of a WC-Co coating is maximum on aluminum substrate and minimum on mild steel substrate. The identical coating exhibits intermediate hardness on titanium substrate.
- The thinner coating has higher hardness than the thicker coating.

Acknowledgments

The author is grateful to DRDO for funding this work through DMR-207. The author is also grateful to Dr. G. Sundararajan, Director, International Advanced Research Centre for Powder Metallurgy and New Materials, for his constant encouragement in preparing this manuscript.

References

1. B. Johnson and S. Hogmark: "Hardness Measurement of Thin Films," *Thin Solid Films*, 1984, *114*, pp. 257-69.
2. P.J. Burnett and D.S. Rickerby: "The Mechanical Properties of Wear Resistant Coatings I: Modelling of Hardness Behavior," *Thin Solid Films*, 1987, *148*, pp. 41-50.
3. S.J. Bull and D.S. Rickerby, "New Developments in the Modelling of the Hardness and Scratch Adhesion of the Thin Films," *Surf. Coat. Technol*., 1990, *42*, pp. 149-64.
4. P.J. Burnett and D.S. Rickerby: "The Mechanical Properties of Wear Resistance Coatings II: Experimental Studies and Interpretation of Hardness," *Thin Solid Films*, 1987, *148*, pp. 51-65.
5. R.S. Montgomery: "Friction and Wear at High Sliding Speeds," *Wear*, 1976, *36*, pp. 275-98.
6. Y. Tirupataiah and G. Sundararajan: "Dynamic Indentation Technique for the Characterisation of the High Strain Rate Plastic Flow Behavior of Ductile Metals and Alloys," *J. Mech. Phys. Solids*, 1991, *39*, pp. 243-71.
7. M.G. Stevenson and P.L.B. Oxley: *Proc. Int. Mech. Eng*., 1970-71, *185*, p. 741.
8. M. Roy, C.V.S. Rao, D.S. Rao, and G. Sundararajan: "Abrasive Wear of Detonation Sprayed WC-Co Coatings," *Surf. Eng*., 1999, *15*, pp. 257-72.
9. Y. Tirupataiah, B. Venkataraman, and G. Sundararajan: "The Nature of the Elastic Rebound of a Hard Ball Impacting on Ductile Metallic Target Materials," *Mater. Sci. Eng*., 1990, *A124*, pp. 133-40.
10. M. Roy, K.P. Rao, S. Joshi, T.P. Bagchi, and G. Sundararajan: *DMRL Technical Report*, DMRL TR92158, Hyderabad, India, 1992.
11. Y. Tirupataiah and G. Sundararajan: "A Comprehensive Analysis of the Static Indentation Process," *Mater. Sci. Eng*., 1987, *A91*, pp. 169-80.
12. H. Ichimura, F.M. Rodriguez, and A. Rodrigo: "A Composite and Film Hardness of TiN Coatings Prepared by Cathodic Arc Evaporation," *Surf. Coat. Technol*., 2000, *127*, pp. 138-43.
13. O.C. Brandt: "Mechanical Properties of HVOF Coatings," *J. Therm. Spray Technol.*, 1995, *4*(2), pp. 147-52.
14. G. Gill: "Investigation on Mechanical Properties of Brittle Wear Resistance Coatings II: Theory," *Thin Solid Films*, 1984, *111*, pp. 201-18.
15. *Metals Handbook,* 10th ed., ASM International, Materials Park, OH, 1990, *2,* p. 978.
16. G. Sundararajan: "An Analysis of the Localization of Deformation and Weight Loss During Single Particle Impact," *Wear*, 1983, *84*, pp. 217-35.
17. G. Sundararajan: "The Saturation of Flow Stress in FCC Metals," *Scr. Metall*., 1982, *16*, pp. 611-14.
18. P. Schemon and G. Sundararajan: in *Annual Review of Material Science*, R.A. Huggins, R.H. Bube, and D.A. Vermilyea, ed., Annual Reviews Inc., CA, 1983, *13*, p. 301.
19. W.D. Mix: "Mechanical Properties of Thin Films," *Metal. Trans*., 1989, *20A*, pp. 2217-45.
20. M. Roy, K.K. Ray, and G. Sundararajan: "An Analysis of the Transition From the Metal Erosion to Oxide Erosion," *Wear*, 1998, *217*, pp. 312-20.
21. D. Tabor: *The Hardness of Metal*, Clarendon, Oxford, UK, 1951.
22. I.M. Hutchings, "Strain Rate Effects in Micro-Particle Impact," *J. Phys. D. Appl. Phys*., 1977, *10*, pp. L179-84.